CHARACTERIZATION OF HORIZONTAL AIR-WATER TWO-PHASE FLOW

R. Kong and S. Kim*
Department of Mechanical and Nuclear Engineering, The Pennsylvania State University
230 Reber Building, University Park, PA 16802, USA
*skim@psu.edu

ABSTRACT

This paper presents experimental studies performed to characterize horizontal air-water two-phase flow in a round pipe with an inner diameter of 38.1mm. A detailed flow visualization study is performed using a high-speed movie camera in a wide range of two-phase flow conditions. Two-phase flows are classified into bubbly, plug, slug, stratified, stratified-wavy, and annular flow regimes. While the transition boundaries identified in the present study compare well with the existing ones in general, some discrepancies are observed for the boundaries of bubbly-to-plug, bubbly-to-slug, and plug-to-slug flows. Two-phase frictional pressure loss analysis is performed using the Lockhart-Martinelli method. For the conditions studied in the present study, it is found that the coefficient C=24 yields the best agreement with the data with the minimum average disagreement. Detailed local experiments are performed in a wide range of conditions in the bubbly flow regime using a four-sensor conductivity probe. An extensive database for local two-phase flow parameters is established, including void fraction, bubble velocity, interfacial area concentration and bubble Sauter mean diameter. Based on this database, functional relations for $\langle\langle v_g \rangle\rangle$ vs. $\langle j \rangle$ and $\langle \alpha \rangle$ vs. $\langle j_g \rangle / \langle j \rangle$ have been studied. It is found that $\langle\langle v_g \rangle\rangle$-$\langle j \rangle$ method predicts the bubble velocity and void fraction better compared to $\langle \alpha \rangle$-$\langle j_g \rangle / \langle j \rangle$ method. Additionally, the evolution of various local two-phase flow parameters in horizontal bubbly two-phase flow is studied by analyzing the measured local parameters along the flow field. Unlike vertical upward bubbly flow, the local void fraction and interfacial area concentration can reach 0.6 and 2000 1/m, respectively, in horizontal bubbly flow. It's noticed that bubbles begin to coalesce near the gas-liquid layer instead of in the highly packed region when gas volumetric flux increases.

KEYWORDS
horizontal two-phase flows, horizontal flow regime, frictional pressure drop, drift flux analysis, local two-phase flow parameters

1. INTRODUCTION

Horizontal two-phase flows are common in many practical engineering applications including nuclear reactors. In a nuclear power system, horizontal two-phase flow occurs in many places such as CANDU reactors accident scenarios. For this reason, understanding horizontal two-phase flow is essential to correctly model the nuclear power system. However, there has been little investigation of horizontal flows compared with vertical flows. The highly asymmetric void distribution in horizontal flow, which is due to the effects of the buoyancy force, adds more difficulties in experimental studies. As such, previous work on vertical flow cannot be directly extended to horizontal flow. Despite this, the closure relations developed for vertical two-phase flow are directly applied to horizontal two-phase flow in nuclear system analysis codes such as TRACE and RELAP. Thus, more work needs to be performed to investigate the interfacial structures of horizontal two-phase flow.

Mandhane et al. [1] developed a flow regime map for gas-liquid flows in horizontal pipes based on a set of experimental data covering a wide range of physical properties and flow parameters. In general, Mandhane's map agrees very well with about 6000 flow conditions. However, few reliable experimental data in bubbly flow leads to the low accuracy in predicting dispersed bubbly flow regime. A theoretical model was developed by Taitel and Dukler [2] to predict flow regime transitions, which took into account the effects of pipe size, fluid properties and angle of inclination. Taitel and Dukler's map shows different transition boundaries in the following respects: (1) transition from bubbly flow to plug/slug flow, (2) transition from slug flow to annular flow, (3) transition from plug flow to stratified flow. Continuous efforts need to be made to investigate the discrepancy.

Lockhart and Martinelli [3] developed a correlation to predict the two-phase frictional pressure drop and the parameter C=20 in the correlation was suggested by Chisholm [4] for the turbulent-turbulent gas-liquid two-phase flow in a straight pipe without flow restrictions. Using the same correlation, Lee and Lee [5] investigated air-water frictional pressure drop in horizontal rectangular channels. The parameter C was newly defined to take account of the channel size and the gas and liquid flow rates. However, less research has been performed to suggest the C value for the horizontal round pipe.

In order to model horizontal two-phase flow phenomena, experimental databases have been established by previous researchers. Kocamustafaogullari and Wang [6] Kocamustafaogullari and Huang [7] and Kocamustafaogullari et al. [8] used a double-sensor conductivity probe to measure local void fraction, interfacial area concentration and bubble Sauter mean diameter in horizontal air-water bubbly flow in a 50.3 mm inner diameter transparent pipe. A linear relationship between $\langle\langle v_g \rangle\rangle$ and $\langle j \rangle$ with a systematic effect of liquid flow was observed. With increasing j_f, the distribution parameter changes from greater than 1to less than 1, and the drift velocity turns from a negative value to a positive value correspondingly. Using all the data, the distribution parameter and drift velocity was found to be 0.99 and -0.09m/s, respectively. Compared with the $\langle\langle v_g \rangle\rangle$ - $\langle j \rangle$ plane, the $\langle \alpha \rangle$-$\langle \beta \rangle$ plane was found to better correlate the data. Talley [9] performed nine test conditions measurements of two-phase parameters using a four-sensor conductivity probe in horizontal air-water two-phase flow in a 38.1 mm transparent pipe, with superficial liquid and gas velocities ranging from 4.00-6.00 m/s and 0.067-0.575 m/s, respectively, at three axial locations (L/D=44, 116, 244) downstream of the two-phase flow injector. The $\langle\langle v_g \rangle\rangle$ - $\langle j \rangle$ plane was found to correlate the data very well with a distribution parameter equal to 1.05 and a drift velocity of -1.23 m/s.

Kocamustafaogullari et al. [8] found that the local and area-averaged void fraction and interfacial area concentration increase with decreasing liquid flow and increasing gas flow in horizontal bubbly flow. The same trend was also observed by Iskandrani and Kojasoy [10] using a hot-film anemometry in a 50.3 mm inner diameter transparent horizontal pipe and by Bottin et al. [11] using an optical probe in a 100 mm inner diameter horizontal pipe.

However, only data taken by the conductivity probe can provide local information on interfacial area concentration which is essential for the closure equations of the two-fluid model. Thus, the database for local measurements of two-phase parameters in horizontal bubbly flow is very limited. Apart from the work done by Talley [9], additional measurements need to be performed to cover horizontal bubbly flow at high gas flow rates.

2. EXPERIMENTAL FACILITY

Experiments are performed in an adiabatic air-water test facility, which is made of 38.1 mm inner diameter, D, clear acrylic pipes, as shown in Fig. 1. The total length of the test section downstream of injector is 9.5m, yielding a development length of 250 diameters. A laser and a digital level are used to ensure the test section is horizontal to within ±0.1 deg. The air flow rate to the test section is measured

through a set of Dwyer Series RMB rotameters with an accuracy of ±3% of the full-scale reading. Two accumulator tanks are placed between the compressor and the two-phase injector in order to reduce the pressure fluctuations in the air. Bubbles are generated by a sintered stainless steel sparger, with an average pore size of 10 μm. Filtered water is supplied to the test section through a 45 kW centrifugal pump, which is stored in an accumulator tank with a capacity of 2,100 liters. The total liquid flow rate is monitored by an electromagnetic flow meter with an accuracy of ±0.5% of the flow rate. The water supply to the test section is split into main (j_{f1}), and auxiliary (j_{f2}) liquid flow rates. The two-phase flow injector has a double annulus configuration. The main liquid flow rate is supplied to the outer annulus and is varied to set the desired test condition. A fixed auxiliary flow is fed to the inner annulus that surrounds the air sparger. This design ensures that bubbles are sheared-off from the sparger surface with a consistent size for all liquid flow rates. Pressure is measured in the test section as shown in Fig.1 by pressure tap using a differential pressure transducer with an accuracy of ±0.01psi.

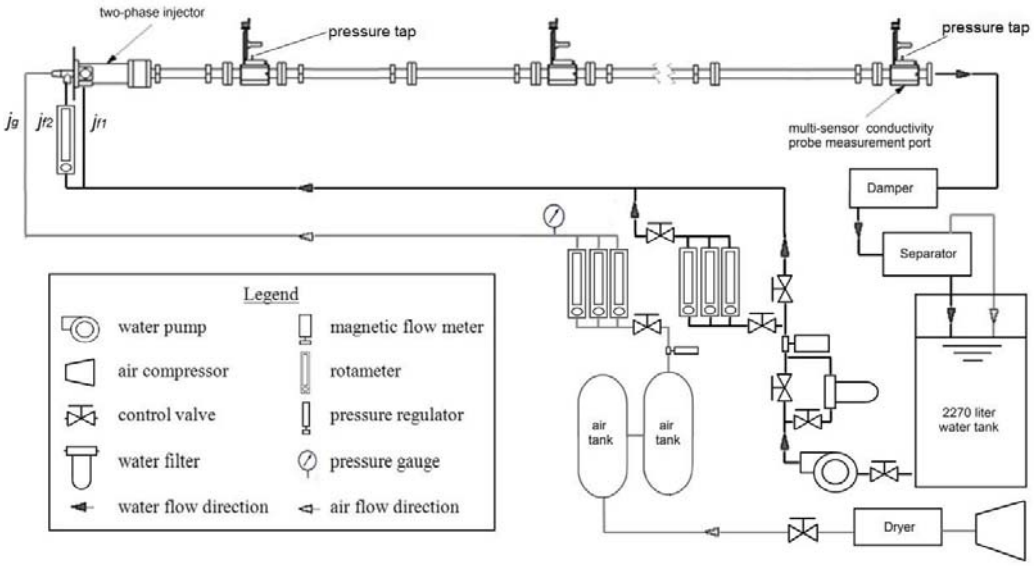

Figure 1. Simplified schematic diagram of the test facility (not to scale).

There are three instrument ports along the test section for multi-sensor conductivity probe measurement, the centers of which are located at L/D=44, 116 and 244 downstream of the two-phase inlet. These ports can also be used for pressure measurements, local conductivity probe measurements and flow visualization studies. To perform flow visualization studies, a high-speed movie camera with a maximum resolution of 512 x 512 pixels is employed. It is capable of 2000 frames per second (fps) provided that the resolution is varied.

The state-of-the-art four-sensor conductivity probe [12] is employed for the measurements of time-averaged local two-phase flow parameters including void fraction α, interfacial area concentration a_i, bubble velocity v_g, bubble frequency f_b and bubble Sauter-mean diameter D_{sm}. A specially designed traversing unit allows the four-sensor conductivity probe to move along the radial direction of the pipe cross-section and to be rotated around the axis of the test section at every 22.5˚in the azimuthal direction without stopping the flow. Considering that the gas distribution in horizontal two-phase flow is asymmetric, such an instrument port is indispensable to obtain the local data throughout the entirety of the flow area. Thus, as shown in Fig. 2, a total of 129 local data points are measured across the entire pipe cross-section. If measurement at 0˚shows symmetry about the vertical axis, data in the second quadrant are copied from the first quadrant.

In this paper, both the flow regime identification and the local conductivity probe measurements will be presented. All twelve test conditions presented in the current study are summarized in Table I, nine of which were taken by Talley [9].

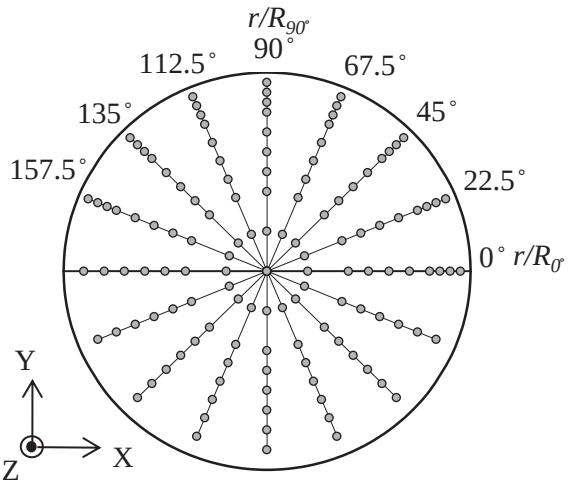

Figure 2. Mesh for measurements of local two phase flow parameters (flow direction is out of the page and the non-dimensional radial distance along an azimuthal angle θ is denoted by r/R_θ.).

Table I. Summary of the test conditions presented in the current study (Runs 1 through 9 were performed by Talley [9])

Run No.	1	2	3	4	5	6	7	8	9	10	11	12
j_f [m/s]	4.00	4.00	5.00	5.00	5.00	6.00	6.00	6.00	6.00	5.00	6.00	5.00
$j_{g,atm}$ [m/s]	0.15	0.25	0.15	0.25	0.50	0.15	0.25	0.50	1.00	0.91	1.84	1.61

3. RESULTS AND DISCUSSION

The discussion of the experimental results is divided into four sections, namely: (1) verification of flow regime transition boundaries, (2) frictional pressure loss analysis, (3) drift-flux analysis, and (4) study on the evolution of various local two-phase flow parameters along the flow field.

3.1. Verification of Flow Regime Transition Boundaries

In order to assess the current horizontal flow regime maps and to improve the accuracy of flow regime prediction in horizontal pipes, a flow visualization study was performed in horizontal air-water two-phase flow. Videos are acquired at an axial location of L/D=244 from the inlet to ensure that the two-phase flow is well developed. The videos are captured by a high speed video camera with different resolution depending on the flow regime. Then, the captured two-phase flow configurations are classified into six conventional horizontal two-phase flow regimes, namely: bubbly, plug, slug, stratified, stratified wavy, annular flow.

In bubbly flow (shown in Fig. 3 (a)), it was observed that liquid Reynolds number (Re_f) play a major role in bubble distribution pattern for a fixed gas flow rate. At low Reynolds number, small near-spherical or

distorted bubbles are concentrated mostly in the upper half portion of the pipe cross-section. As Re_f becomes larger, on the other hand, bubbles start to get distributed across the entire pipe cross-section.

In plug flow (shown in Fig. 3 (b)), elongated gas plugs move in the upper half portion of the pipe with an asymmetric round nose. Unlike the slug flow, the plug flow is characterized by plug bubbles with thinly elongated tails, followed by liquid regions with few dispersed bubbles present.

In slug flow (shown in Fig. 3 (c)), gas slug bubbles move with a higher velocity than the small bubbles in the lower half portion of the pipe. It is characterized by gas slugs with blunt tails followed by a distinct liquid slug containing a lot of small bubbles. It can be also observed in the slug flow that the rotation of bubble clusters as shown in Fig. 3 (c) is present on the order of the gas slug depth in the wake region.

In stratified flow (shown in Fig. 3 (d)), gas phase is separated from liquid phase and is flowing in the upper portion of the pipe while liquid flows in the lower portion of the pipe. Smooth interface without disturbances is present between the two phases. The only difference between stratified flow and stratified-wavy flow (shown in Fig. 3 (e)) is the appearance of disturbances at the interface between the two phases.

In Annular flow (shown in Fig. 3 (f)), a continuous gas core is present with a liquid film around the periphery of the pipe. The liquid film is rough and wavy, and is thicker at lower portion of the pipe. Dispersed liquid droplets entrained from the liquid film can be also observed in the gas core.

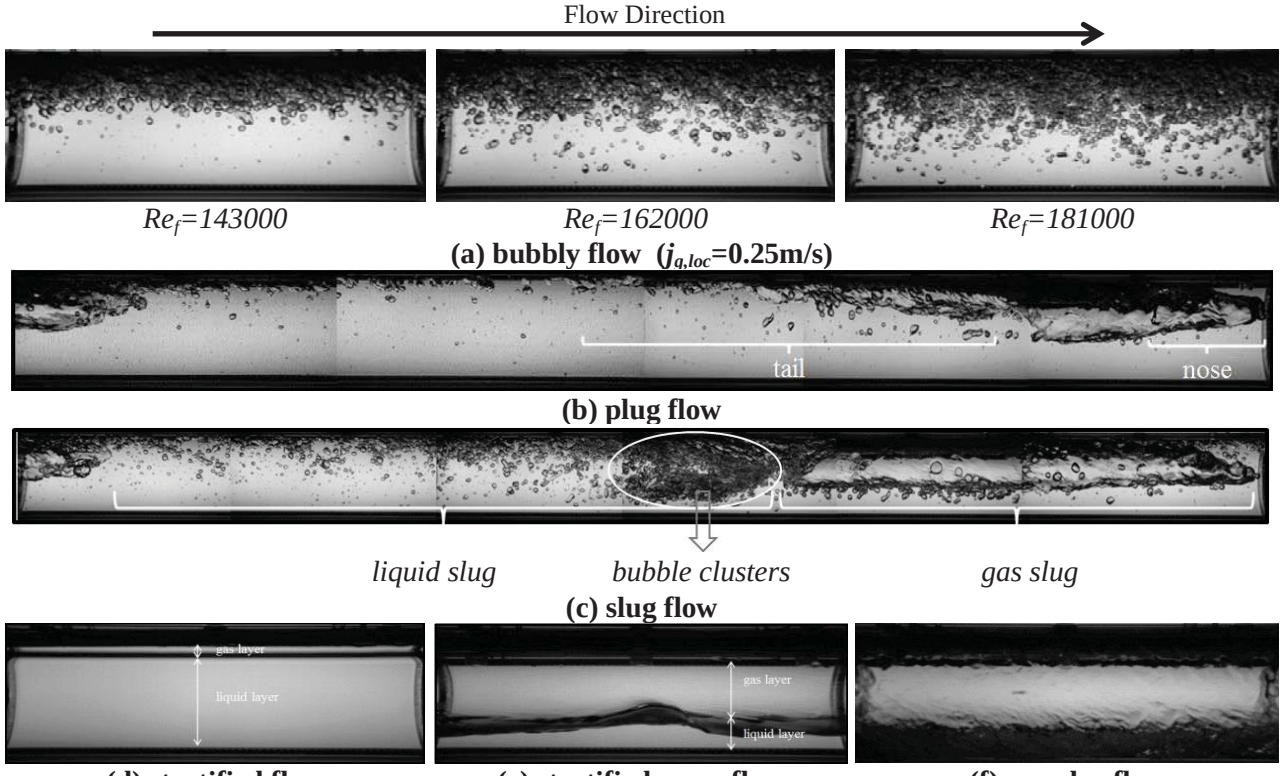

Figure 3. Examples of image of horizontal air-water two-phase flow regimes.

In total, videos of 263 flow conditions are taken to span bubbly/plug/slug/stratified/stratified wavy flows as shown in Fig. 4. In order to mitigate subjectivity in deriving boundaries between flow regimes, these videos are viewed and classified by multiple independent researchers. In Fig. 5, newly derived regime

transition boundaries in the present study are shown together with the flow regime boundaries suggested by Mandhane et al. [1]. It is found that the new transition boundaries generally agree well with Mandhane's map. Disagreement also occurs, however, at the transition from bubbly- to-plug and bubbly-to-slug flows. In Mandhane's map, transitions occur at a constant liquid volumetric flux of j_f=4.00 m/s regardless of the gas volumetric flux. However, the new result suggests that the transition may be dependent on the gas volumetric flux. As such, at lower gas volumetric flux, transition occurs at a lower liquid volumetric flux. Additionally, a discrepancy can be also found at the transition from plug flow to slug flow at high liquid flow rates. The boundary observed in the present study suggests that it may require more gas to make transition from plug to slug at a liquid volumetric flux of less than 1 m/s, and require less gas with a liquid volumetric flux of above 1 m/s. This finding is opposite to that by Mandhane et al. [1] but more physical in that, as the liquid flow becomes more turbulent, the transition from plug to slug is promoted requiring less gas.

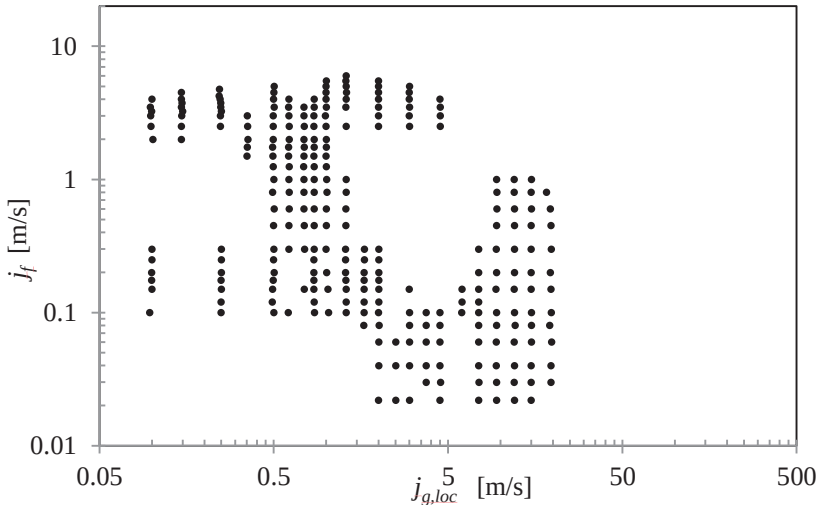

Figure 4. Experimental test conditions for flow visualization.

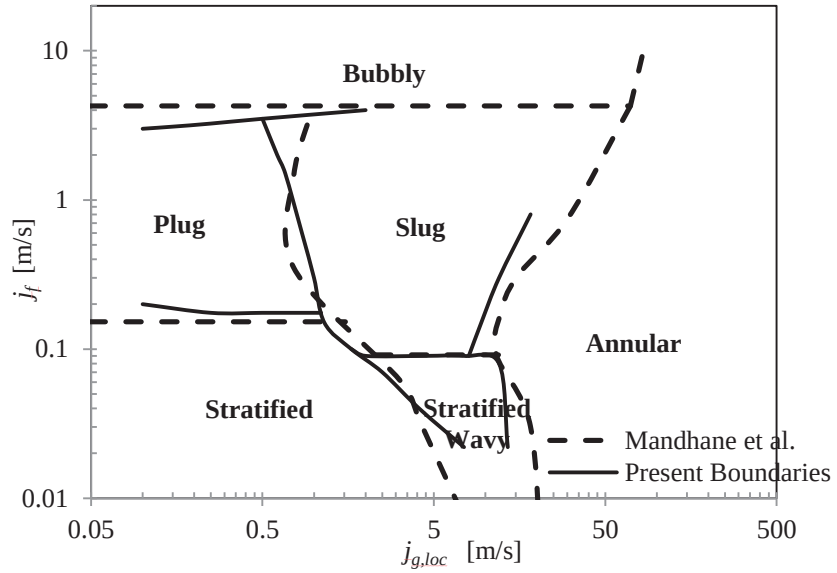

Figure 5. Comparison between present boundaries and Mandhane et al. [1].

3.2. Frictional Pressure Loss Analysis

The frictional pressure drop in horizontal air-water two-phase flow is predicted using the approach of Lockhart and Martinelli [3], which assumes that the two-phase frictional pressure drop is the summation of pressure drop caused by each phase and the interaction between two phases given by

$$\phi_f^2 = 1 + \frac{C}{X} + \frac{1}{X^2} \tag{1}$$

where ϕ_f^2 and X, are the two-phase frictional multiplier and Martinelli parameter, respectively, defined by:

$\phi_f^2 \equiv \frac{(dp/dz)_F^{2\emptyset}}{(dp/dz)_F^f}$ and $X^2 \equiv \frac{(dp/dz)_F^f}{(dp/dz)_F^g}$

Here, the frictional loss for each phase is obtained by:

$$(\frac{dp}{dz})_F^k = \frac{2f}{D}\rho_k j_k^2 \tag{2}$$

where f, D, ρ, and j denote the friction factor, pipe diameter, density, and superficial velocity, respectively. The subscript k denotes the liquid or gas phase index of f or g. The friction factor for turbulent flow is obtained using Blasius formulation given by:

$$f = 0.079(\frac{\rho_k j_k D}{\mu_k})^{-0.25} \tag{3}$$

The pressure drop in two-phase flow can be estimated by finding an appropriate parameter C in Eq. (1). In horizontal bubbly flow, the transport of dispersed gas bubbles is driven by the liquid flow, which is highly turbulent in all of the present experimental conditions. Based on the data acquired in the present study in a wide range of bubbly flow regime, C=24 is found to give the best fit to experimental data with an average percent difference of ±1.10%, while C=20 gives ±1.40% as shown in Fig. 6.

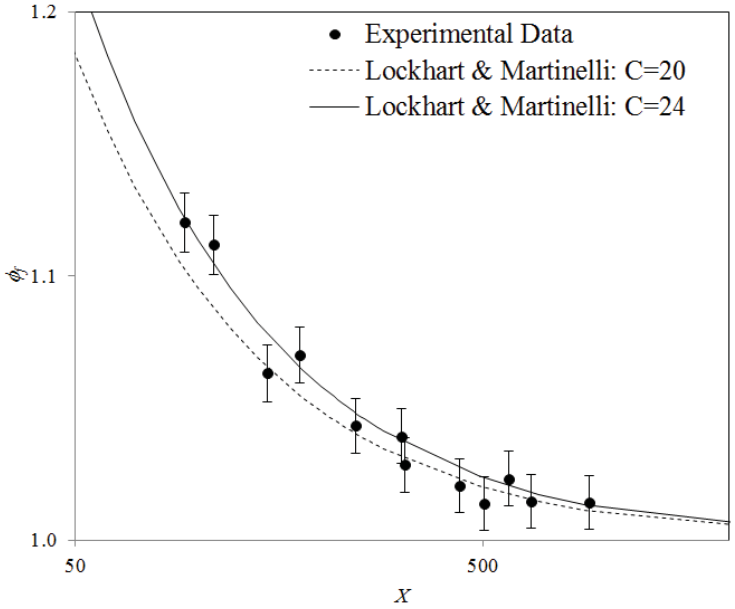

Figure 6. Predicted two-phase multiplier using Lockhart-Martinelli approach (±1% error bars).

3.3. Interfacial Structure in Horizontal Air-water Two-phase Flow

To gain confidence with the four-sensor conductivity probe measurements, superficial gas velocity at each port determined from the probe measurements ($<\alpha v_g>$) is benchmarked with that based on gas rotameter and pressure measurements ($j_{g,loc}$). As shown in Fig. 7, a good agreement is found between the two measurements yielding an average percent difference of ±5.3%.

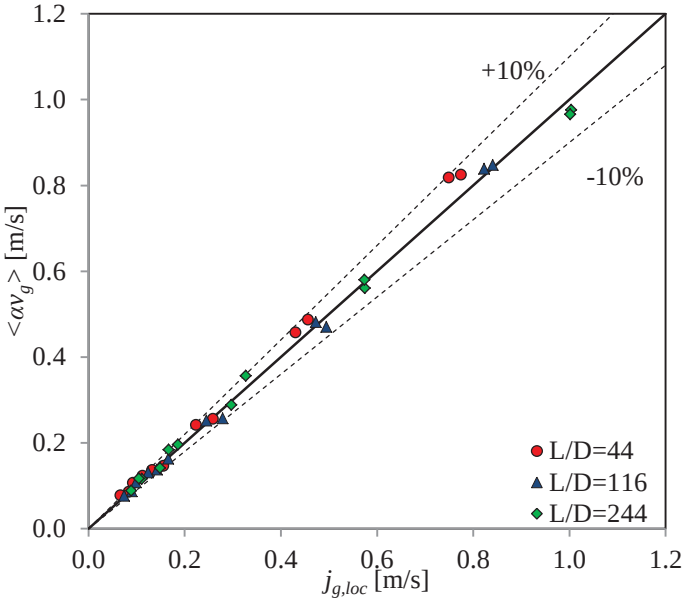

Figure 7. Benchmark of four-sensor conductivity probe measurement for $<\alpha v_g>$ versus $j_{g,loc}$.

3.3.1. Drift-flux analysis

In view of the practical applications towards two-phase flow analysis, the one-dimension relationship between $\langle\langle v_g \rangle\rangle$ and $\langle j \rangle$ (Zuber and Findlay [13]) provides a convenient way to furnish closure models, which can be obtained from local conductivity probe and flow rotameters, respectively. The conventional $\langle\langle v_g \rangle\rangle$-$\langle j \rangle$ formulation is given by:

$$\langle\langle v_g \rangle\rangle = \frac{\langle j_{g,loc} \rangle}{\langle \alpha \rangle} = C_0 \langle j \rangle + \langle\langle V_{gj} \rangle\rangle \tag{4}$$

where C_0 is the distribution parameter and $\langle\langle V_{gj} \rangle\rangle$ is the drift velocity defined as:

$$C_0 = \frac{\langle \alpha j \rangle}{\langle \alpha \rangle \langle j \rangle} \tag{5}$$

$$\langle\langle V_{gj} \rangle\rangle = \frac{\langle \alpha v_{gj} \rangle}{\langle \alpha \rangle} \tag{6}$$

where $\langle j \rangle$ is the total superficial velocity given by:

$$\langle j \rangle = \langle j_f \rangle + \langle j_{g,loc} \rangle \tag{7}$$

Here, the subscript "loc" denotes the superficial gas velocity evaluated at a given axial location. $\langle \quad \rangle$ and $\langle\langle \quad \rangle\rangle$ represent the area-averaged quantity over a cross-sectional area and the void-weighted area-averaged quantity, respectively. With experimentally acquired $\langle\langle v_g \rangle\rangle$, $\langle \alpha \rangle$, $\langle j_f \rangle$ and $\langle j_{g,loc} \rangle$, a linear relationship is found between $\langle\langle v_g \rangle\rangle$ and $\langle j \rangle$ as shown in Fig. 8 (a). Most of the data agree well with one relationship without exhibiting the effect of liquid flow rate observed by Kocamustafaogullari et al. [8]. The values of C_0 and $\langle\langle V_{gj} \rangle\rangle$ are determined to be 1.05 and -1.21 m/s, respectively. The significantly negative drift velocity indicates that gas phase moves slower than liquid phase in horizontal flow. Apart from the relationship between $\langle\langle v_g \rangle\rangle$ and $\langle j \rangle$, the $\langle \alpha \rangle$-$\langle \beta \rangle$ plane (Zuber and Findlay [13]) is also used to analyze the experimental data. This approach can be used to predict the area-averaged void fraction. Eq. (4) can be expressed as:

$$\langle \alpha \rangle = \frac{\langle \beta \rangle}{C_0 + \dfrac{\langle\langle V_{gj} \rangle\rangle}{\langle j \rangle}} \tag{8}$$

where $\langle \beta \rangle$ is given by:

$$\langle \beta \rangle = \frac{\langle j_{g,loc} \rangle}{\langle j \rangle} \tag{9}$$

The linear relationship between $\langle \alpha \rangle$ and $\langle \beta \rangle$, as shown in Fig. 8 (b), suggests that C_0+$\langle\langle V_{gj} \rangle\rangle/\langle j \rangle$ is a nearly constant value. From the slope of the plot, this value is determined to be 0.85. Moreover, C_0+$\langle\langle V_{gj} \rangle\rangle/\langle j \rangle$ can also be calculated using the results of C_0 and $\langle\langle V_{gj} \rangle\rangle$ obtained from $\langle\langle v_g \rangle\rangle$-$\langle j \rangle$ plane. This value for each test conditions is found to be within ±3.6% of the average value, which is 0.83. This indicates that constant C_0+$\langle\langle V_{gj} \rangle\rangle/\langle j \rangle$ for horizontal bubbly flow is an acceptable hypothesis.

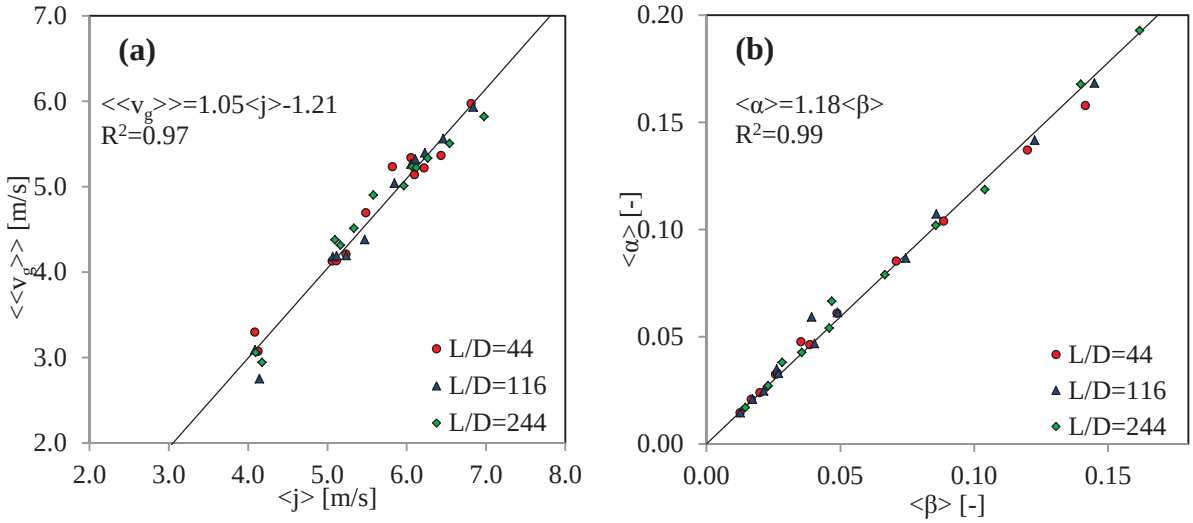

Figure 8. Relationship of (a) $\langle\langle v_g \rangle\rangle$-$\langle j \rangle$ and (b) $\langle \alpha \rangle$-$\langle \beta \rangle$ in horizontal bubbly flow.

Based on the $\langle\langle v_g \rangle\rangle$-$\langle j \rangle$ plot, $\langle\langle v_g \rangle\rangle$ can be correlated with $\langle j \rangle$ by:

$$\langle\langle v_g\rangle\rangle = 1.05\langle j\rangle - 1.21 \tag{10}$$

Noting that$\langle\langle v_g\rangle\rangle$=$\langle j_{g,loc}\rangle/\langle\alpha\rangle$ and $\langle j_{g,loc}\rangle$ can be obtained from flow measurements, void fraction $\langle\alpha\rangle$ can be estimated by Eq. (10). The comparison of measured and predicted values of $\langle\langle v_g\rangle\rangle$ and $\langle\alpha\rangle$ is shown in Fig.9. This approach predicts the data very well, with an average disagreement of ±2.7% for bubble velocity and ±2.7% for void fraction.

As a comparison, the void fraction and bubble velocity are predicted from the $\langle\alpha\rangle$-$\langle\beta\rangle$ plot by:

$$\langle\alpha\rangle = 1.18\frac{\langle j_{g,loc}\rangle}{\langle j\rangle} \tag{11}$$

$$\langle\langle v_g\rangle\rangle = \frac{\langle j_f\rangle}{1.18 - \langle\alpha\rangle} \tag{12}$$

Comparison of measured and predicted values of $\langle\langle v_g\rangle\rangle$ and $\langle\alpha\rangle$ is shown in Fig.10. This approach performs well with a disagreement of ±4.9% for bubble velocity and ±4.2% for void fraction, although not better than the previous approach. This result is different from that by Kocamustafaogullari et al. [8] due to the significantly negative drift velocity in the present study.

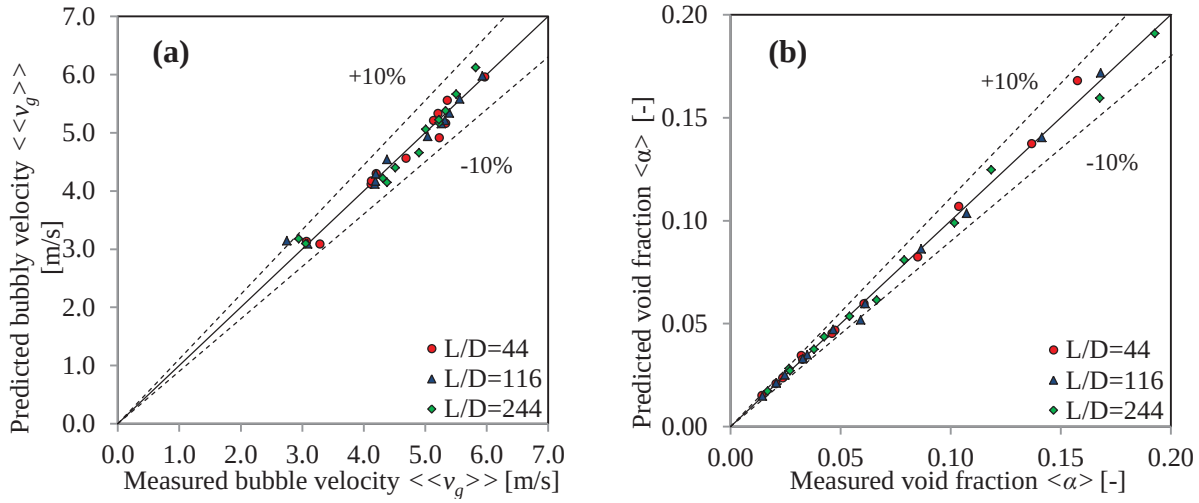

Figure 9. Comparison of measured and predicted (a) $\langle\langle v_g\rangle\rangle$ and (b) $\langle\alpha\rangle$ by $\langle\langle v_g\rangle\rangle$-$\langle j\rangle$ plane.

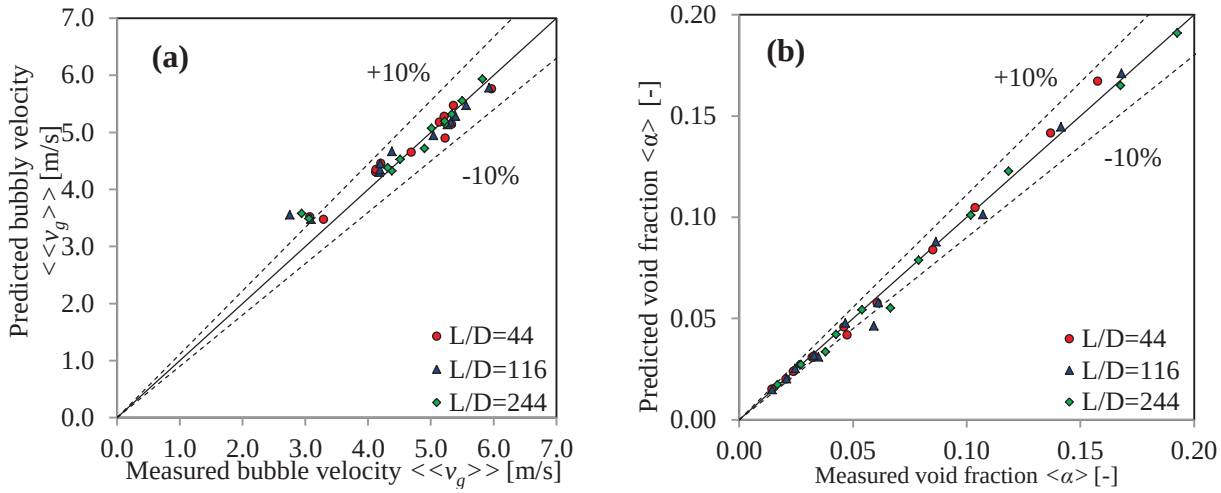

Figure 10. Comparison of measured and predicted (a) $\langle\langle v_g \rangle\rangle$ and (b) $\langle\alpha\rangle$ by $\langle\alpha\rangle$-$\langle\beta\rangle$ plane.

3.3.2. Study on the evolution of various local two-phase flow parameters along the field

The effects of gas and liquid volumetric flux on various local two-phase flow parameters such as void fraction, interfacial area concentration, bubble diameter and bubble velocity are investigated in this section.

All of the surface plots (i.e. Fig. 11) of the measured local void fraction are generated using MATLAB. The ability to obtain such detailed local information is due to the four-sensor conductivity probe traversing and rotating mechanism without interrupting the experiment. Because α and a_i show a similar distribution in the bubbly flow regime, only the profiles of α are shown here. In the figures, r/R denotes probe radial position with positive values at upper (or right) and negative values at lower (or left) region of the pipe cross section. The subscripts V and H denote the vertical axis and horizontal axis, respectively.

The effect of increasing $j_{g,loc}$ on void fraction distribution for a fixed j_f is shown in Fig. 11. As shown in the figures, bubbles migrate to the upper portion of the pipe due to the buoyancy force. With increasing $j_{g,loc}$, both the peak and the area-averaged values of void fraction increase. Unlike vertical upward bubbly flow, the peak values of α and a_i can reach up to approximately 0.6 and 2000 1/m, respectively, in horizontal bubbly flow. Similar trend was reported by Kocamustafaogullari and Wang [6]. The effects of increasing $j_{g,loc}$ on Sauter mean diameter and bubble velocity for a fixed j_f are shown in Fig. 12. It's observed that the D_{sm} and v_g exhibit power law behavior. The bubble size is largest near the center of the pipe, and decreases towards the wall. Increasing $j_{g,loc}$ slightly increases the bubble size due to coalescence. This suggests that most of the bubble coalescences happen near the gas-liquid layer instead of in the highly packed region when transition happens from bubbly flow to plug or slug flow. Bubbles tend to move at higher velocity in the lower portion of the pipe. Increasing $j_{g,loc}$ shows different effects on bubble velocity in different regions. When $r/R > 0.7$, increasing $j_{g,loc}$ decreases bubble velocity while opposite effect is observed when $r/R < 0.7$. This is because gas phase follows liquid phase in horizontal bubbly flow and densely packed bubbles provide strong resistance to the motion of liquid. Higher gas flow rates introduce more resistance to the liquid, thus the liquid phase moves slower at $r/R > 0.7$. Correspondingly, the liquid phase moves faster at $r/R < 0.7$ due to continuity.

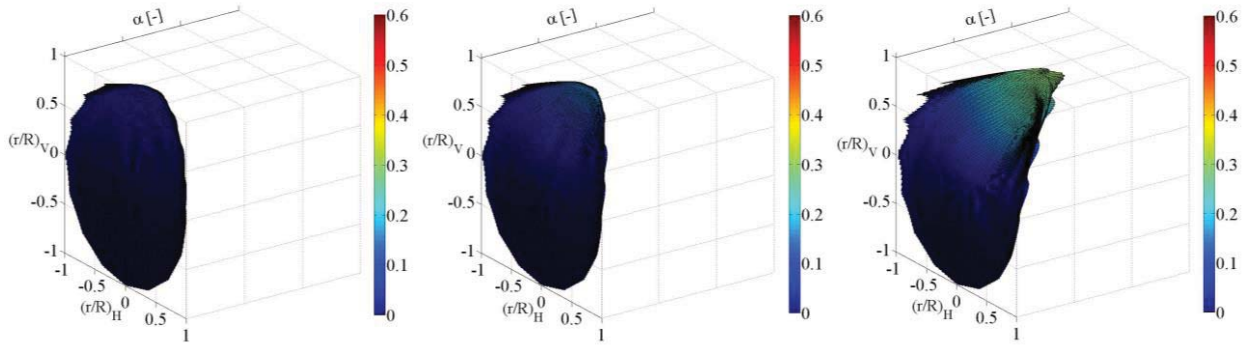

(a) $j_{g,loc}$=0.105m/s, <α>=0.027 (b) $j_{g,loc}$=0.167m/s, <α>=0.043 (c) $j_{g,loc}$=0.327m/s, <α>=0.079

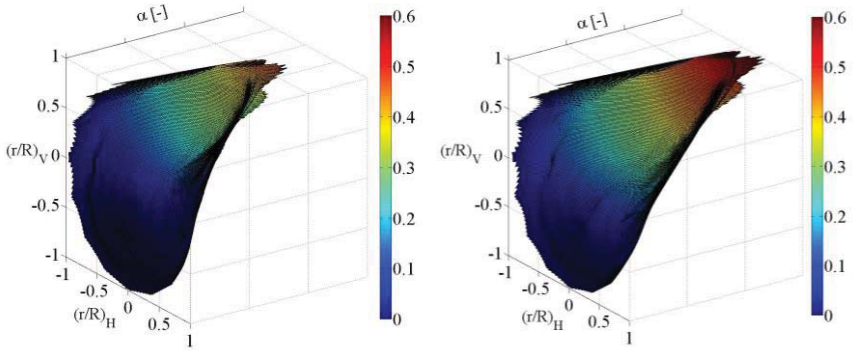

(d) $j_{g,loc}$=0.576m/s <α>=0.118 (e) $j_{g,loc}$=1.612m/s <α>=0.193

Figure 11. Effect of $j_{g,loc}$ on α for j_f =5.00m/s at L/D=244.

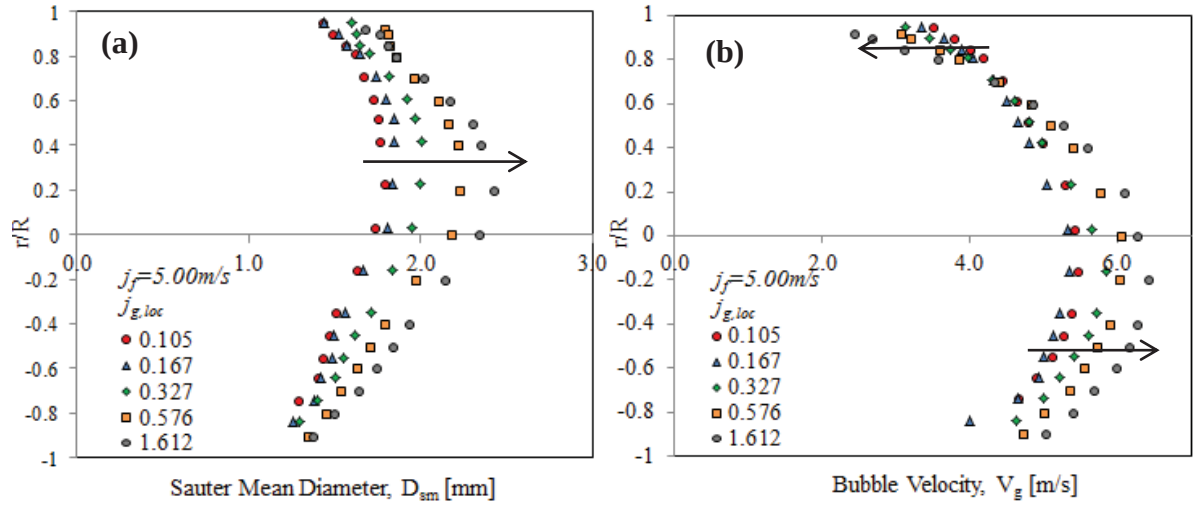

Figure 12. Effect of $j_{g,loc}$ on (a) D_{sm} and (b) v_g for j_f =5.00m/s at L/D=244 of vertical axis (90°), arrows denote trend with increasing $j_{g,loc}$.

The effects of increasing j_f on void fraction distribution, bubble Sauter mean diameter and bubble velocity for a fixed $j_{g,atm}$ are shown in Fig. 13. Increasing j_f decreases the peak and area-averaged values of void fraction. Bubbles are more distributed to the lower portion of the pipe which is confirmed by the observation that no bubbles are detected when r/R< -0.2 at the lowest j_f. Increasing j_f promotes bubble

breakup due to increased turbulence. Increased system pressure at higher j_f also causes bubble Sauter mean diameter to decrease. Bubbles move faster at higher j_f, which confirms that gas phase follow liquid phase in horizontal bubbly flow.

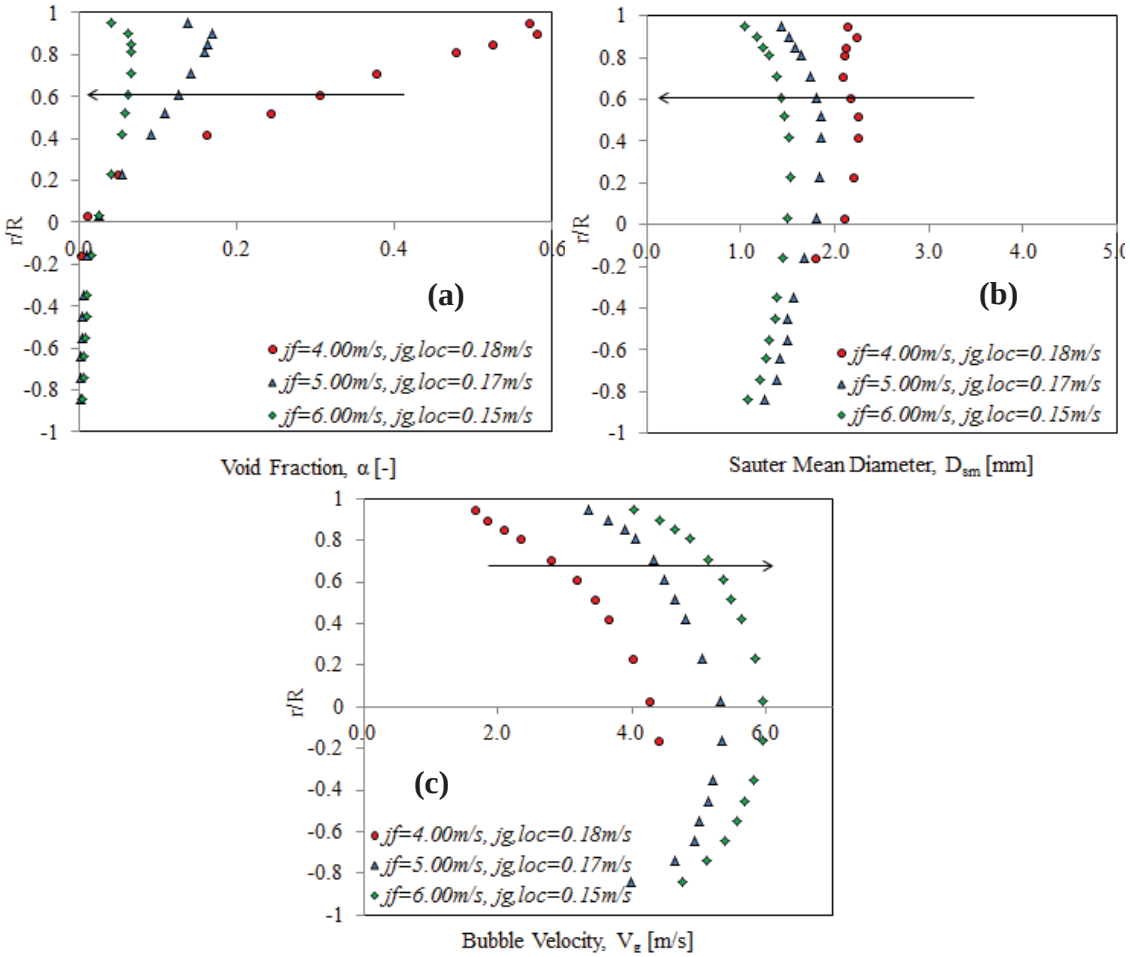

Figure 13. Effect of j_f on (a) α, (b) D_{sm} and (c) v_g for $j_{g,atm}$=0.25m/s at L/D=244 of vertical axis (90˚), arrows denote trend with increasing j_f.

4. CONCLUSIONS

Experiments are performed to characterize horizontal air-water two-phase flow. In order to verify the existing flow regime transition boundaries for horizontal two-phase flow, a detailed flow visualization study is performed using a high-speed movie camera for a total of 262 flow conditions, which are classified into bubbly, plug, slug, stratified, stratified-wavy, and annular flow. It's found that the present transition boundaries compare well with the existing ones, in general. Differences are observed at the transitions from bubbly-to-plug and bubbly-to-slug flow. Also, a discrepancy is shown at the transition from plug flow to slug flow.

The frictional pressure loss in horizontal bubbly flow is predicted using Lockhart-Martinelli method. For all the twelve conditions studied in this paper, the coefficient C=24 is found to give the best agreement with the data with the minimum percent difference of ±1.10%.

In order to characterize the transport of two-phase flow in horizontal pipe, a four-sensor conductivity probe is used to obtain local two-phase flow parameters in horizontal bubbly flow. Based on this database, the drift-flux analysis is performed using both the $\langle\langle v_g \rangle\rangle$ vs. $\langle j \rangle$ relationship and the $\langle \alpha \rangle$ vs. $\langle j_g \rangle / \langle j \rangle$ relationship. In the first approach, the distribution parameter C_0 and the drift velocity $\langle\langle V_{gj} \rangle\rangle$ are found to be 1.05 and -1.21 m/s, respectively. The significantly negative drift velocity indicates that the gas phase moves slower than the liquid phase in horizontal bubbly flow. In the second method, a constant value of 0.85 is found for $C_0+\langle\langle V_{gj} \rangle\rangle / \langle j \rangle$ from the slope of the plot. It's found that $\langle\langle v_g \rangle\rangle$-$\langle j \rangle$ better predicts bubble velocity and void fraction.

The evolution of various local two-phase flow parameters in horizontal bubbly two-phase flow is studied by analyzing the measured local parameters along the flow field. Unlike vertical upward bubbly flow, the local void fraction and interfacial area concentration can reach 0.6 and 2000 1/m, respectively, in horizontal bubbly flow. With increasing gas volumetric flux, most of the bubbles coalescences happen near the gas-liquid layer instead of in the highly packed region. Bubbles are found to move faster in the lower region of the pipe while opposite effect is observed in the higher region when gas volumetric flux increases. Bubbles are more distributed to the lower portion of the pipe when liquid volumetric flux increases. It's also found that increasing liquid volumetric flux promotes bubble breakup and leads to bubble Sauter mean diameter decrease.

REFERENCES

1. J. M. Mandhane, G. A. Gregory, and K. Aziz, "A flow pattern map for gas—liquid flow in horizontal pipes," *International journal of multiphase flow,* **1**, pp. 537-553 (1974).
2. Y. Taitel, and A. E. Dukler, "A model for predicting flow regime transitions in horizontal and near horizontal gas-liquid flow," *AIChE Journal,* **22**, pp. 47-55 (1976).
3. R. W. Lockhart, and R.C. Martinelli, "Proposed correlation of data for isothermal two-phase, two-component flow in pipes," *Chem. Eng. Prog.,* **45**, pp. 39-48 (1949).
4. D. Chisholm, "A theoretical basis for the Lockhart-Martinelli correlation for two-phase flow," *International journal of heat and mass transfer,* **10**, pp. 1767-1778 (1967).
5. H. J. Lee, and S. Y. Lee, "Pressure drop correlations for two-phase flow within horizontal rectangular channels with small heights," *International Journal of Multiphase Flow,* **27(**5), pp. 783-796 (2001).
6. G. Kocamustafaogullari, and Z. Wang, "An experimental study on local interfacial parameters in a horizontal bubbly two-phase flow," *International journal of multiphase flow,* **17**, pp. 553-572 (1991).
7. G. Kocamustafaogullari, and W. D. Huang, "Internal structure and interfacial velocity development for bubbly two-phase flow," *Nuclear engineering and design,* **151**, pp. 79-101 (1994).
8. G. Kocamustafaogullari, W. D. Huang, and J. Razi, "Measurement and modeling of average void fraction, bubble size and interfacial area," *Nuclear engineering and design,* **148**, pp. 437-453 (1994).
9. J. D Talley, "*Interfacial area transport equation for vertical and horizontal bubbly flows and its application to the TRACE code*," THE PENNSYLVANIA STATE UNIVERSITY (2012).
10. A. Iskandrani, and G. Kojasoy, "Local void fraction and velocity field description in horizontal bubbly flow," *Nuclear engineering and design,* **204**, pp. 117-128 (2001).
11. M. Bottin, J. P. Berlandis, E. Hervieu, M. Lance, M. Marchand, O. C. Öztürk, and G. Serre, "Experimental Investigation of a Developing Two-Phase Bubbly Flow in Horizontal Pipe," *International Journal of Multiphase Flow*, **60**, pp. 161-179 (2014).
12. S. Kim, X. Y. Fu, X. Wang, and M. Ishii, "Development of the miniaturized four-sensor conductivity probe and the signal processing scheme," *International journal of heat and mass transfer,* **43**, pp. 4101-4118 (2000).
13. N. Zuber, and J. A. Findlay, "Average volumetric concentration in two-phase flow systems," *Journal of Heat Transfer,* **87**, pp. 453-468 (1965).